Scanning Microscopy

Volume 5 | Number 4 Article 2

10-28-1991

Surface Topographical and Compositional Characterization Using Backscattered Electron Methods

Dirk A. Wassink
University of Michigan

Jerry Z. Raski
IBM

Joel A. Levitt
Ford Scientific Research Laboratory

David Hildreth
University of Michigan

Kenneth C. Ludema
University of Michigan

Scanning Microscopy, Vol. 5, No. 4, 1991 (Pages 919-926) 0891-7035/91$3.00+.00
Scanning Microscopy International, Chicago (AMF O'Hare), IL 60666 USA

SURFACE TOPOGRAPHICAL AND COMPOSITIONAL CHARACTERIZATION USING BACKSCATTERED ELECTRON METHODS

Dirk A. Wassink[1], Jerry Z. Raski[2], Joel A. Levitt[3], David Hildreth[1], Kenneth C Ludema[1,*]

[1]Mechanical Engg. Dept., University of Michigan, G.G. Brown Building, Ann Arbor, MI 48109-2125
[2]IBM, MS DS 255/57-1, 1701 North Street, Endicott, NY 13760
[3] Ford Scientific Research Laboratory, PO Box 2053, Dearborn, MI 48121

(Received for publication May 10, 1991, and in revised form October 28, 1991)

Abstract

Two pairs of diametrically opposed Schottky surface barrier diodes in a modified scanning electron microscope (SEM) are used to reconstruct surface elevations and composition differences. An empirically determined function of difference of signals from opposing diodes is used to calculate slopes, which are then integrated to elevations by an efficient 2-dimensional Fast Fourier Transform. Composition differences are distinguished by variations in the overall backscattered electron (BSE) intensity estimated by the sum of the four diode signals. Arithmetic average roughness measurements from the BSE device are within 10% of stylus surface tracer measurements when surface slopes average less than 6 degrees and maximum slopes are less than 45°; shadowing effects for rough surfaces, aliasing, and averaging effects from Fourier integration are apparent. Composition measurements show distinction of high contrast phases; phase boundary-slope interactions are noted.

Key Words: backscattered electrons, surface roughness, surface phase, Lambertian angular distribution, Schottky surface barrier diodes, partial slopes, two-dimensional fast Fourier transform, magnetic deflection distortion, electron beam blanking, aliasing.

***Address for correspondence**:
Kenneth C Ludema
University of Michigan,
Mechanical Engineering Department,
G.G. Brown Building,
Ann Arbor, MI 48109-2125

Phone: 313/764-3364
FAX: 313/747-3170

Introduction

This paper describes the development and validation of a method for simultaneously mapping material phase and topography of a solid surface, using backscattered electrons (BSE).

Several workers have used BSE to quantify surface topography or material composition. Lebiedzik [5-7] used BSE and secondary electrons (SE) to reconstruct topography over a grid. Reimer, Bongeler and Desai [10] used BSE to quantify topography on a line scan. In each case difference signals were used to estimate slope, and integration was carried out to obtain elevations. Carlsen [2] and Sato and O-hori [12] have suggested methods for integrating slope data. Carlsen applied trapezoidal integration over an entire grid of slope data, using least squares averaging and relaxation methods. His integration averages over many paths, requiring much time. Sato and O-hori integrate along the data collection path, thus reducing integration time but leaving large errors in single measurements [12]. Ball and McCartney [1] and Robinson, Cutmore, and Burdon [11] utilize BSE signals from a high take-off angle detector above the specimen to estimate its apparent atomic number.

Scanning electron microscopes (SEM) which measure BSE to reconstruct topography have major advantages over conventional devices for measuring surface topography. For example, the electron beams used in the modified SEM can be focused to a spot size of 10 nm, enabling better resolution potential than the commonly used stylus surface tracer, which has a tip radius 1000 times as large. Further, measurements with SEM do not plastically deform the surface. The problem with such devices has been to convert high resolution in terms of spot size into quantitative resolution of surface elevations, i.e. topography. If, in addition, compositional differences can be mapped simultaneously with topography, then the location of phase boundaries can be known with higher precision than if separate or successive maps of phase and position are used to characterize surfaces.

A signal processing system was designed using four Schottky surface barrier surface diodes to be placed in an existing SEM. Raski completed mathematical modeling for this system and built it, installing it in a scanning electron microscope [8].

Method

Measurement of BSE

Four ORTEC TA-019-100-100 Schottky barrier diodes arranged as two diametrically opposed pairs, are located just below the final lens in the column of a modified SEM at

Table 1. List of symbols.

Symbol	Meaning
x,y	Calibrated estimate of true beam position
Xs,Ys	Nominal beam position (neglect distortion)
Sx,Sy	Scanning sensitivities in x and y directions
Vx,Vy	Scan control voltages
dx,dy	Polynomial functions describing magnetic distortion
Vi	Amplified voltage signal from ith diode
I_B	Primary beam current
I_{bse}	BSE current
h	Elevation of detector array above specimen
ξ	Take-off angle of detectors
ζ	Angle between surface normal and scatter direction
η	Backscatter coefficient, the ratio of backscatter current to primary beam current
Mi	Position compensated diode signal of ith diode
Si	Position compensated, normalized difference signal

Table 2. Data for Schottky surface barrier diodes.

Parameter	Pair 1	Pair 2
Nominal area	100 mm^2	100 mm^2
Nominal Resistivity	1400 Ohm cm	2500 Ohm cm
Specific Capacitance	6.0 pF/mm^2	4.5 pF/mm^2
Max Stopping Energy	50 keV	59 keV
Depletion Layer Depth	18 μm	22 μm
Threshold energy	3.58 keV	3.58 keV

take-off angles of 45° from the z-axis as shown in Figure 1. A list of symbols is given in Table 1. Data for the diodes is given in Table 2.

Since the exact gains of the diodes and amplifying circuits are likely to be imperfectly balanced, the relative gains of opposing diodes is measured. The electron beam is positioned near the center of the scan field, and measurements from the diodes with the fixture in one position are compared with those after a 180° rotation of the diode fixture. The relative gains of the two pairs are also computed.

Nominally, the SEM electron beam is positioned at scan coordinates (X_S,Y_S) by x- and y-control voltages V_X and V_Y, such that

$$(X_S,Y_S)=(S_XV_X,S_YV_Y), \qquad (1)$$

where S_X and Sy are the positioning sensitivities in the x- and y-directions. Because of the aberrations present in magnetic lenses and scanning systems the sensitivities are not constant, and the coordinates of the true beam position (x,y) may be described by equation (2),

$$x = S_xV_x + dx(X_S,Y_S)$$
$$y = S_yV_y + dy(X_S,Y_S) \qquad (2a,b)$$

where dx and dy are polynomial functions of magnetic deflection distortion from location (Xs,Ys), the first order coordinates of the spot. In view of the magnetic deflection distortion, a calibration procedure was developed to compute the aberrations dx and dy in the form of a seven term, third-order polynomial corresponding to the representation by Haantjes and Lubben [4]. The aberration function is then used to compensate signals sent to position the electron beam.

In addition, synchronous detection with 2 kHz electron beam blanking is utilized, to eliminate the "sag" in the diodes described by Frost, Harrowfield, and Zuiderwyk [3], and to remove DC coupling from the detection system. The amplification circuitry integrates the signal positively while the beam is on the specimen, and negatively during beam blanking such that constant noise signals are effectively cancelled out.

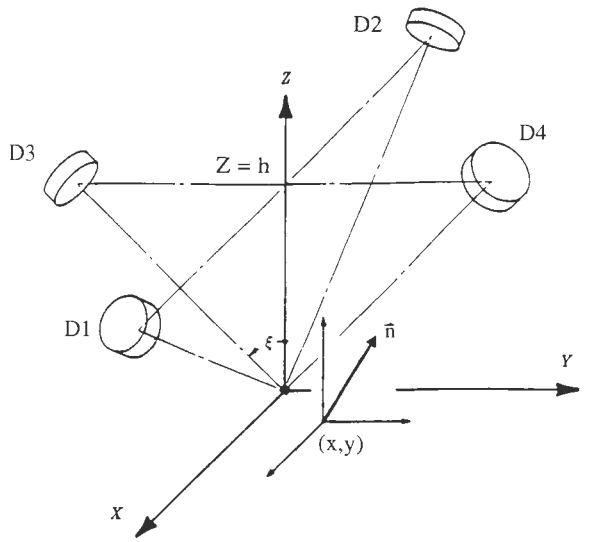

Figure 1. Geometric notation for measured point (x,y) in a four diode detection system. Take-off angle of detectors is ξ=45°. Z=h=21.121mm.

Intensities from the four diodes are collected pointwise over a 64 by 64 point square and stored for further analysis. The grid size is limited mainly by computer storage capability; it is desired to make larger grids than 64 by 64, because there is no obvious way to connect separate grids.

Topographical reconstruction

Partial slopes at each measurement point may be determined from the BSE intensities measured by the four diodes; these in turn are integrated into elevations using a two-dimensional Fast Fourier technique.

Calculation of partial slopes. The partial slopes in the x and y-directions can be obtained from the differences in current in opposing diodes, using equations which account for the geometry of the detectors and the position of the electron beam. The topography reconstruction technique [9] was originally based on the assumption that measured BSE distribution about the surface normal for the range of slopes to be measured would be Lambertian. The backscatter current varies with the cosines of angle between the surface normal and scattering direction, ζ; that is, $dI_{bse}/d\Omega=I_B\cos(\zeta)/\pi)$, where dI_{bse} is the backscatter current for a differential solid angle Ω, and I_B is the primary beam current.

The signal incident on each of the BSE detectors depends on the angle between the surface normal and the line from the measured point to the detector and the distance from the measured point to the detector. Since the angle is the variable of interest, the effect of the distance from detector to measurement point must be removed. With knowledge of the expected detector signal for a given surface orientation, the surface partial derivatives can be reconstructed. First define position-compensated detector signals to compensate for the positions of sampling point and detectors (Eq. 3a-d).

$$M_1 \equiv \frac{\pi V_1}{I_{bse}} \frac{[(h\tan(\xi) - x)^2 + y^2 + h^2]^2}{[h\tan(\xi) - x]\sin(\xi) + h\cos(\xi)} \quad (3a)$$

$$M_2 \equiv \frac{\pi V_2}{I_{bse}} \frac{[(h\tan(\xi) + x)^2 + y^2 + h^2]^2}{[h\tan(\xi) + x]\sin(\xi) + h\cos(\xi)} \quad (3b)$$

$$M_3 \equiv \frac{\pi V_3}{I_{bse}} \frac{[(h\tan(\xi) - y)^2 + y^2 + h^2]^2}{[h\tan(\xi) - y]\sin(\xi) + h\cos(\xi)} \quad (3c)$$

$$M_4 \equiv \frac{\pi V_4}{I_{bse}} \frac{[(h\tan(\xi) + y)^2 + y^2 + h^2]^2}{[h\tan(\xi) + y]\sin(\xi) + h\cos(\xi)} \quad (3d)$$

The variables of Eq. (3) are as follows: Vi is the amplified voltage signal from the ith diode, I_{bse} is the backscatter current, h is the elevation of the detector array above the specimen, and ξ=45° is the take-off angle of the detectors. The parameters S_1 and S_2, given in Equation (4a,b) are the position-compensated, normalized detector difference signals.

$$S_1 \equiv \frac{M_1 - M_2}{M_1 + M_2} \qquad S_2 \equiv \frac{M_3 - M_4}{M_3 + M_4} \quad (4a,b)$$

The x- and y-partial derivatives are then

$$\frac{\partial z}{\partial x} = \frac{hS_1}{h\tan(\xi) + xS_1 + yS_2} \quad (5a)$$

$$\frac{\partial z}{\partial y} = \frac{hS_2}{h\tan(\xi) + xS_1 + yS_2} \quad (5b)$$

Near (x,y) = (0,0) these relations reduce to Equations (6a,b) which compare well with Lebiedzik's empirical results for small slopes, which are not compensated for beam position.

$$\frac{\partial z}{\partial x} \approx \frac{V_1 - V_2}{V_1 + V_2} \qquad \frac{\partial z}{\partial y} \approx \frac{V_3 - V_4}{V_3 + V_4} \quad (6a,b)$$

However, for measurements taken from standard surfaces (sphere, roughness standard) the analytical model based on a Lambertian distribution fails to give slopes corresponding to those expected from specimen geometry. The Lambertian distribution of BSE applies to the energy spectrum as a whole, but Schottky diodes record a signal which is proportional to the energy of BSE; thus, they measure the BSE distribution with sensitivity skewed toward high energy BSE. Since the distribution of high-energy BSE is different from that of the low-energy BSE, and variation in BSE distribution with energy is complex, the functions

$$\frac{\partial z}{\partial x} = \text{ftn}\left(\frac{hS_1}{h\tan(\xi) + xS_1 + yS_2}\right) \quad (7a)$$

$$\frac{\partial z}{\partial y} = \text{ftn}\left(\frac{hS_2}{h\tan(\xi) + xS_1 + yS_2}\right) \quad (7b)$$

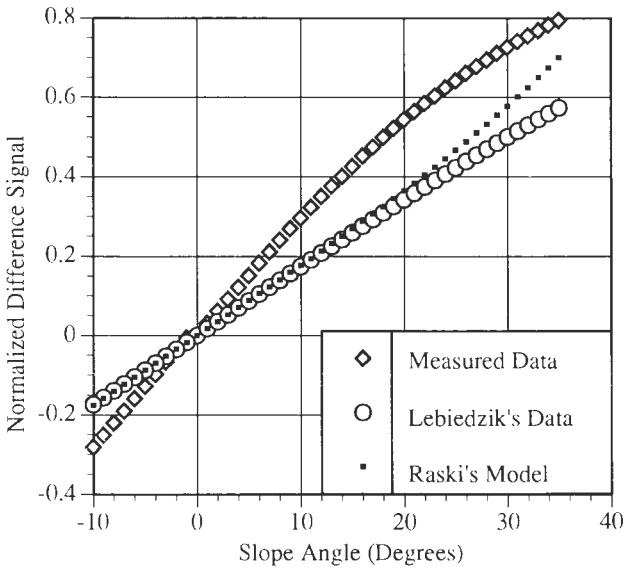

Figure 2a. Models and data describing x-variation of normalized difference signal with slope.

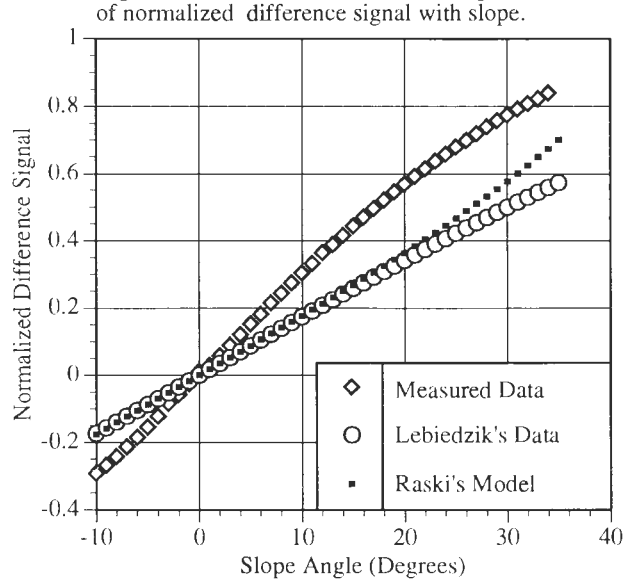

Figure 2b. Models and data describing y-variation of normalized difference signal with slope.

were measured empirically using a smooth, medium atomic number specimen (chromium). Results for measurements at the origin (x,y)=(0,0) are compared with Lebiedzik's (in which the difference signal is proportional to the sine of the slope angle) and Raski's analytical results (where the difference signal is proportional to the tangent of the slope angle) in Figure 2. The functions (7a,b) have been incorporated into Raski's analysis. The slopes calculated by this method then are independent of incident beam current and overall backscattering coefficient, η.

In summary, the electron beam is positioned precisely at each measurement point through use of the compensation function for magnetic distortion at that point. BSE signals from each detector are compensated for the position of measurement on the specimen with respect to detector geometry using Eq. (3a-d). Slope is then determined from the compensated detector signals using Eq. (4) and the empirical functions shown in Figures 2a and 2b.

Integration of slopes. The partial derivatives are then integrated using a two-dimensional Fast Fourier Transform (2D-FFT) method developed by Raski et al. [9]. This method makes use of a 4x4 vector radix to reduce the amount of computation in integrating the slopes while retaining much of the accuracy. Elevations at each point are reconstructed separately from x and y partial derivatives and averaged together after integration. The resulting array of elevations is then plotted as a series of two dimensional traces which represent the surface. Integrating in Fourier transform space cannot be done until all measurements for a field of study have been taken, so this method is not as quick as that of Sato and O-hori (integration along measurement path only) [12]. It also does not give the extensive averaging of Carlsen's method [2], but the compromise of speed and averaging gives fairly precise results in a reasonable amount of time.

Composition Mapping

The signal from a BSE detector increases approximately monotonically with the atomic number of the measured specimen, although it is not necessarily a precise representation of the overall backscatter yield, η. This variation applies when surfaces are measured at the same, small tilt, and when operating conditions are the same.

In the SEM, the sum of the signals from the four semiconductor detectors is used to detect compositional changes on a specimen surface. Since topographical variations are present largely in the difference signals of the pairs of diodes, such variations are largely eliminated by summation of the signals. In order to minimize variations over a scanned surface, the BSE intensities measured by the four diodes are normalized with respect to beam position, and with respect to the relative sensitivities of the diodes. If the incident beam is kept constant during the measurement time, the variations in the sum signal can be used to characterize compositional changes on a specimen.

Measured intensity values are only proportional (as a first approximation) to the backscattering coefficient; the proportionality constant is not known. If specimen current and primary beam current were measured in addition to BSE intensity, an empirical equation could be used to estimate the apparent atomic number of each phase. Such an estimate would be enhanced by the addition of a high take-off angle, large solid angle detector placed under the pole piece of the final lens.

Experimental Results

The following two sections describe features and artifacts of surface topographical and compositional maps. In Figures 3 through 7, surface elevations are shown in graphical form, and BSE intensity or composition differences are distinguished by line thickness. Unless otherwise stated, successively higher intensities are indicated by successively thinner lines. Primary beam current used for measurements was in the range 1.0-3.0 nanoamperes (nA).

First, a well characterized specimen was examined: a silicon specimen overlaid with a gold lattice.. In Figure 3, a combined map of BSE intensity and topography of this specimen shows clear distinction of gold (high atomic number Z, high backscatter yield η) and silicon (low Z, low

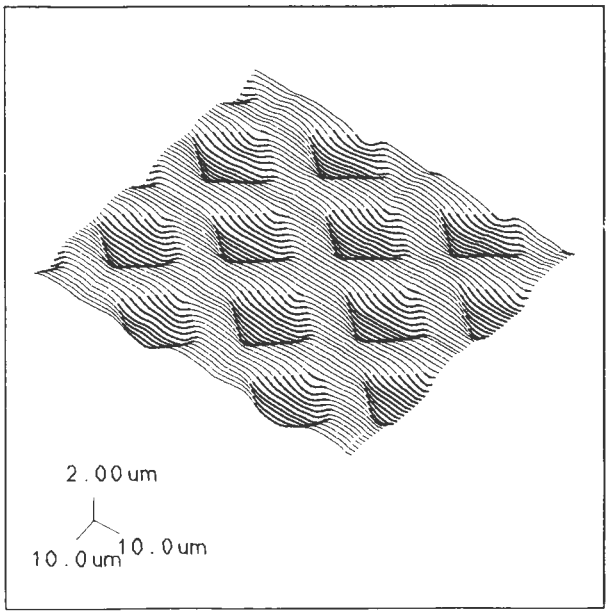

Figure 3. Combined BSE intensity and topography map of a gold lattice (thin lines) on a silicon substrate (thick lines).

η). Although the slopes between the gold lattice and silicon base layer have been prepared to be nearly 90°, the measured slopes are not greater than the measuring limit of 45°. The map shows correspondingly gentler slopes between the phases. Edge effects may contribute to this phenomenon.

Next, a study was done on gray cast iron specimens of varying surface roughness to test topography and phase interactions. Five specimens of different roughness were examined; in addition to polished and fractured specimens, cast iron ground with #600, #320, and #180 grinding paper were used (Figure 4). In the polished specimen, graphite flakes were clearly distinguished from the pearlite matrix. With successively rougher surfaces, regions of ferrite and graphite were still clear, as were topographical features resulting from grinding or fracture. Calculated length-average roughness (R_a) from BSE data was 0.577μm, compared with stylus tracer measurements with the same sampling length, which averaged 0.452μm and ranged from 0.406μm to 0.597μm. The 30% discrepancy between BSE calculated roughness and tracer average roughness may be explained from the microstructure of gray cast iron: the narrow channels where graphite has been removed during specimen cleaning are too narrow for the tracer stylus tip to reach the bottom.

Silicon carbide coated with approximately 25nm of gold/palladium was examined (Figure 5; note that the thick lines represent higher BSE intensity for this figure.). Topography shows quite clearly the cavities on the surface formed by removal of whole grains from the surface. In addition, a second phase of small particles with high BSE intensity is shown on the surface. The specimen was examined by x-ray analysis, and these particles were found to contain large amounts of tungsten. Most likely the particles have been left behind during the original grinding of the silicon carbide with tungsten carbide.

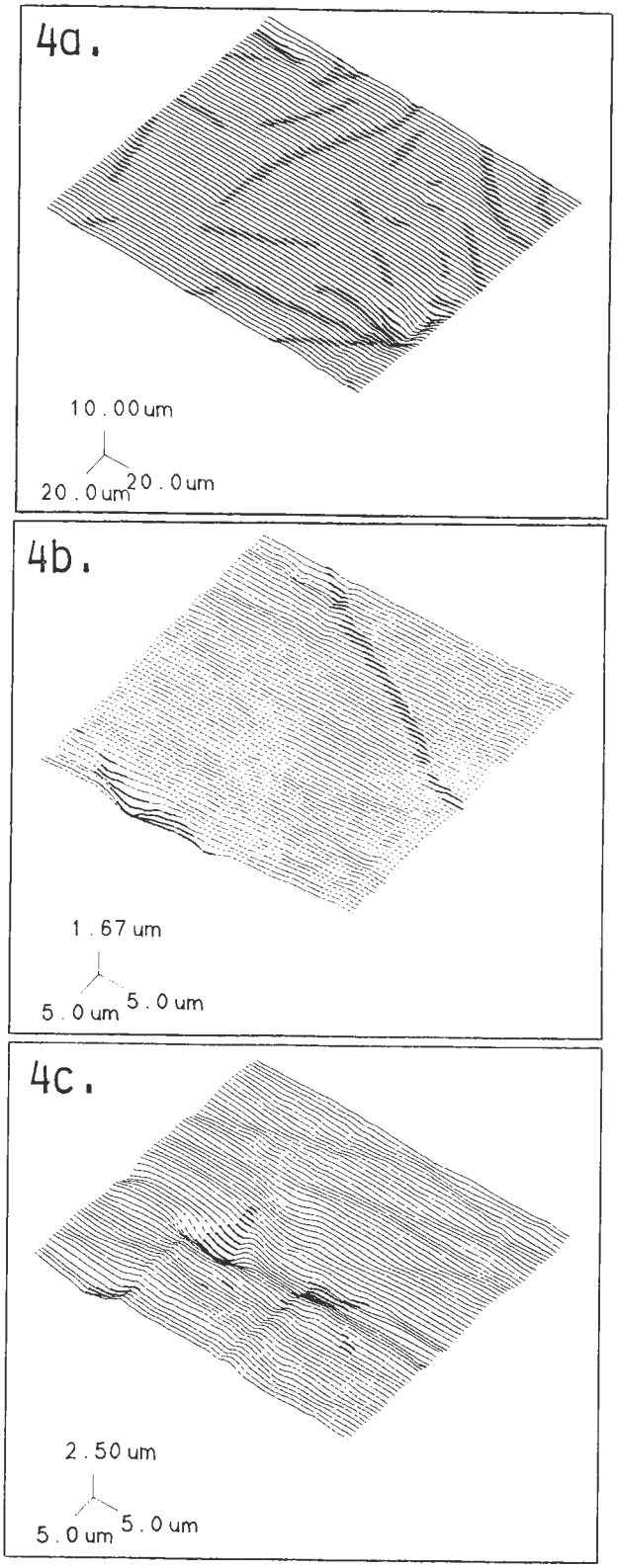

Figure 4. Combined BSE intensity and topography maps of gray cast iron (pearlite, thin lines; graphite, thick lines) with various degrees of surface finishing: a) polished; b) ground to #600 grit; c) ground to #320 grit; d) ground to #180 grit; e) fractured surface.

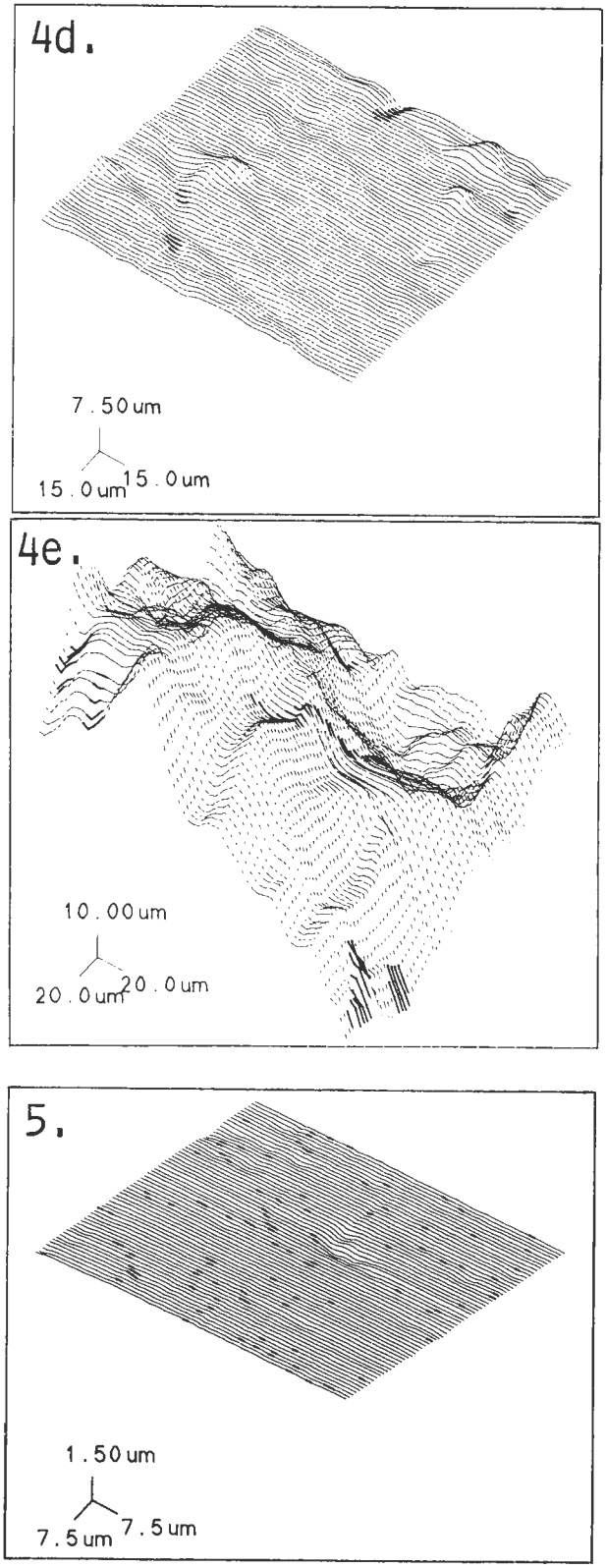

Figure 5. Combined BSE intensity and topography map of silicon carbide, showing tungsten impurities from manufacturing. (Silicon carbide, thin lines; tungsten, thick lines)

Problems and Artifacts

Background noise

In order to test background noise in the BSE instrument a smooth, flat chromium surface was measured. A plot of the elevations of the chrome surface calculated by the method outlined above showed that the surface is quite flat for normal vertical scale amplification. However, measured elevational variations of up to 0.1μm are present in the form of ripples aligned with the grid axes. Some elevational variation due to surface imperfections and noise are to be expected, but the regular form of the variation in the measurements suggests that the Fourier integration method distributes the effect of surface imperfections by averaging the perturbations out along orthogonal paths. This averaging effect will also be noted later for a dust particle on a surface.

Shadowing

It was expected that shadowing effects might vary with the severity of surface roughness. A series of steel specimens of varying surface roughness was examined to determine the maximum measurable slope for the system. Roughness calculated for a specimen of #180 grit ground steel was 0.347μm, within 10% of the average (0.385μm) of measurements taken using a stylus tracer. This specimen had an average slope of 6°. The calculated roughness of specimens with lower average slope compared similarly to surface tracer measurements. The steepest slope measured was 45°, which occured on a fractured steel surface. This maximum measured slope results only when one diode of an opposing pair has a signal of zero, while the other diode has some non-zero value; this corresponds with complete shading. Examination of the fractured steel specimen in an optical microscope indicated that the surface had much steeper slopes than were measured. Shadowing effects could be compensated as suggested by Reimer, Bongeler, and Desai [10].

Slope effects on phase measurement

Slope is derived from the difference between BSE signals of opposing diodes divided by the sum of the same signals. According to detector array geometry, some variation in total BSE intensity with slope would be expected, even for a flat homogeneous specimen. A tilt with an oblique azimuth might produce a different total intensity than a tilt with azimuth aligned with the diode axes. Measurements taken on a sphere in the range of +/- 20° slope indicated that the influence of slope on BSE intensity is insignificant for this range. In addition, measurements on a specimen of fractured gray cast iron appear to resolve graphite flakes despite the presence of slopes of 45° and greater.

Beam Current Variations

One additional note should be made concerning phase resolution with the BSE device. Primary beam current fluctuations, due for example to misalignment of the apertures or lenses or filament aging, can cause fluctuations in measured BSE intensity. Since the primary beam current is not considered in the BSE intensity calculations, any variation will appear directly in the values of intensity used to distinguish phase. As an example of this, BSE data was taken on a smooth specimen when the SEM column and final aperture were misaligned. The primary beam current varied from about 0.5nA, where the lowest BSE intensities were measured, to about 3.0nA, where the highest BSE intensities were measured. The result, shown in Figure 6, is a variation in BSE intensity across the field of study. This effect reduces the ability of the BSE device to distinguish phases. However, variations in primary beam current were found to be negligible for normal running conditions.

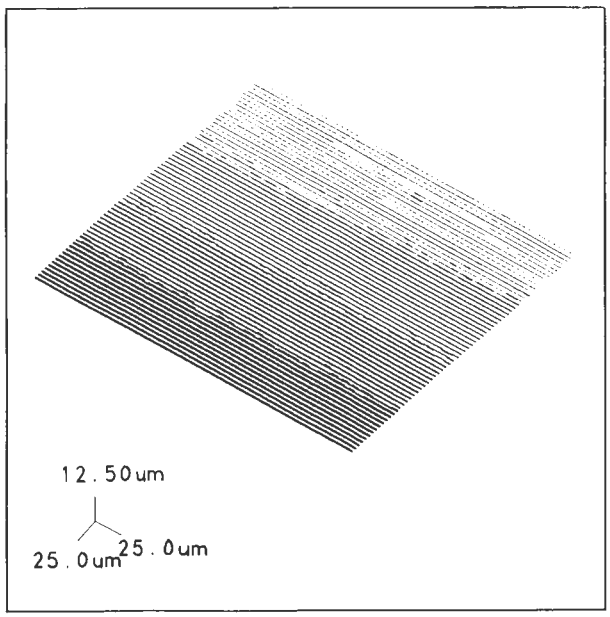

Figure 6. Variation of BSE intensity across a scan field of a smooth chromium specimen caused by electron beam fluctuation from misalignment of SEM column. Thickest lines represent lowest BSE intensity, with successively higher intensities given by stepwise thinner lines.

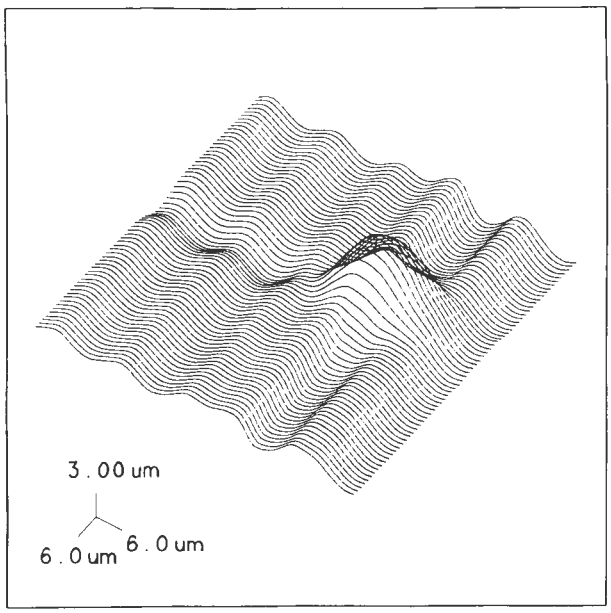

Figure 7. Measured topography of roughness standard with dust particle. Note disturbances extending across the scan field in orthogonal directions from dust particle. Unattached dust particle is shown as attached because slopes greater than 45° are measured as 45°.

Unattached particles

An elevation map showing a roughness standard with a dust particle on its surface is shown in Figure 7. Not only is the dust particle represented as continuous with the surface (because of the inability of the BSE device to measure angles greater than 45 degrees), but the surface features around the dust particle become distorted. The distortion appears in two

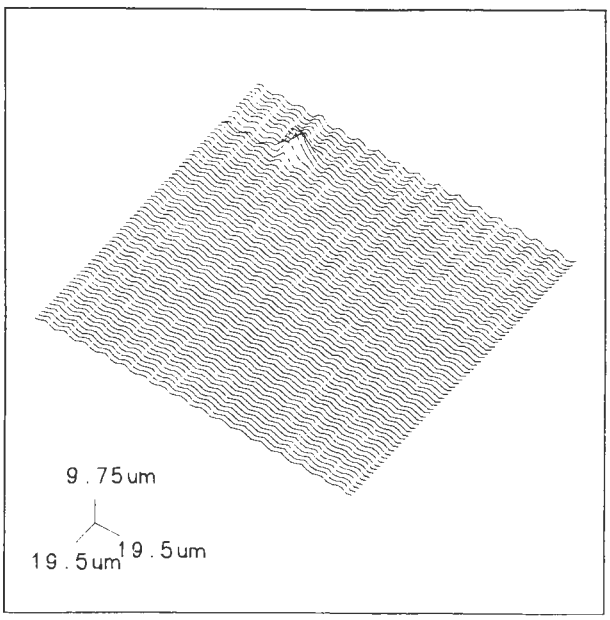

Figure 8. Lower magnification topographical map of specimen in Figure 7 shows a smaller disturbance from the dust particle. Note that ribs of the roughness standard appear somewhat jagged; this is the result of aliasing.

orthogonal directions aligned with the sides of the data field. This distortion is not well understood, but could be a result of averaging effects from the FFT technique used to obtain surface elevations from slopes.

Aliasing

Discrete measurements such as those used in constructing BSE topography and phase maps will produce erroneous results if the spaces between measurements are larger than features of interest on the measured surface. By application of the sampling theorem for signal processing, sample spacing must be smaller than one-half of the size of surface features to be measured. On a roughness standard sample it was observed that a sample spacing close to the size of the ribs showed the features as jagged (Figure 8). A cross-sectional study of the roughness standard showed it to have periodically alternating parallel ridges and grooves, for which the radius of curvature of the grooves is greater than that of the peaks. Calculated roughness for this specimen was 18% higher than stylus tracer measurements.

In addition, the diameter of the beam should be approximately equal to the sample spacing, so that a measurement represents the *average* slope between the previous and next measurement points. Aliasing is noted where the focus of electron beam is much smaller than the sample spacing. Calculations of roughness for a roughness standard varied up to 60% when focus of the electron beam was varied over a wide range. Careful manual focusing reduced this variation in roughness calculations values to within 10% of stylus tracer measurements. Methods for automatic focusing may be employed to adjust the beam diameter to a size appropriate for a given sample spacing.

Phase boundary slope

An abrupt phase boundary crossed during BSE slope measurement may cause some distortion in slope measurement. If the beam rests on the boundary between a low Z material and a high Z material, then an artificial slope may be measured as a result of the varying backscattering behavior of the two materials. The "lopsidedness" of backscattering should be a function of the angle of the interface between the phases with respect to the specimen surface. Hence, in measurements of multiphase materials (e.g. gray cast iron), we must be careful to distinguish where possible whether slopes at material interfaces are caused by real topography (i.e. from preferential wear of a softer phase, or material removal) or as an artifact of the calculation procedure. Monte Carlo modelling of this effect may enable compensation for its effects.

Conclusions

The simultaneous mapping of topography and material composition by backscattered electrons is a promising approach to microsurface characterization. At present, the topography of surfaces with average slopes less than six degrees and maximum slopes less than 45° can be reproduced quantitatively to a precision of 10%. Simultaneous mapping of topography and material phase has been demonstrated for high contrast material combinations. The measurements are subject to the following limitations: 1) topographical measurements are sensitive to beam focus; 2) phases are resolved by differences in BSE intensity, so atomic number is not calculated.

Acknowledgement

The authors wish to acknowledge the donation of the silicon and gold specimen to this project by Michel S. Michail of IBM Corporation, East Fishkill Facility.

References

1. Ball MD, McCartney DG. (1981). The measurement of atomic number and composition in an SEM using backscattered electrons. J. Microsc. **124**: (Part I) 57-68.

2. Carlsen IC. (1985). Reconstruction of true surface topographies in scanning electron microscopes using backscattered electrons. Scanning **7**: 169-177.

3. Frost MT, Harrowfield IR, Zuiderwyk M. (1981). A Wide Bandwidth, Solid State BSE Detector for the SEM and Microprobe. J. Phys. E: Sci. Instrum. **14**: 597-601.

4. Haantjes J, Lubben RG. (1957). Errors of Magnetic Deflection, I. Philips Res. Rep. **12**: 46-48.

5. Lebiedzik J, White EW. (1975) Multiple Detector Method for Quantitative Determination of Microtopography in the SEM. Scanning Electron Microsc. **1975**: 181-188.

6. Lebiedzik J. (1975). Multiple Electron Detector Method for Quantitative Microtopographic Characterization in the SEM. Ph.D. Thesis. Pennsylvania State University, University Park, PA.

7. Lebiedzik J. (1979). An Automatic Topographical Surface Reconstruction in the SEM. Scanning **2**: 230-237.

8. Raski JZ. (1986). The Measurement of Texture using Backscattered Electrons. Ph.D. Thesis. University of Michigan, Ann Arbor, MI.

9. Raski JZ, Levitt JA, Ludema KC. (1988). Surface topography from Back-scattered Electron Data using a Noise-reducing Fourier Method. Surface Topography **1**: 397-414.

10. Reimer L, Bongeler R, Desai V. (1987). Shape from Shading using Multiple Detector Signals in Scanning Electron Microscopy. Scanning Microsc. **1**: 963-973.

11. Robinson VNE, Cutmore NG, Burdon RG. (1984). Quantitative composition analysis using the back-scattered electron signal in a scanning electron microscope. Scanning Electron Microsc. **1984**;II: 483-492.

12. Sato H, O-hori, M. (1987). Surface roughness measurement using scanning electron microscope with digital processing. ASME Jour: Eng. for Industry **109**: 106.

Discussion with Reviewers

V.N.E. Robinson: The use of smaller diodes would give greater accuracy, at least as far as dimensions are concerned.
O.C. Wells: It is known that the angular distribution with which backscattered electrons leave a sample is not always a cosine distribution. For example, from a single crystal the angular distribution is covered with peaks and lines caused by electron channeling effects.

For years now David Dingley at the University of Bristol in England has been demonstrating the use of a fluorescent screen and a television system (that has now been computerized) to give images showing the angular distribution with which BSE leave a solid target. Such a viewing system can be expected to show cutoff effects caused by the local inclination of the specimen and much else that would be invaluable in this situation.
Authors: If the electron beam diameter is smaller than the grain size of the surface under study, channeling effects may be significant. The detectors used have been chosen somewhat larger than might be prudent purely for dimensional accuracy in order to obtain sufficient signal-to-noise ratios to resolve a 0.1 milliradian change in slope. The larger detectors have the added benefit of averaging out channeling peaks.

V.N.E. Robinson: Several researchers have shown that the BSE signal contains almost no topography when the high take-off angle BSEs are detected. It would be possible to measure atomic number purely from one small detector placed around the incident beam.
O.C. Wells: It puzzles me as to why the authors restrict themselves to only four BSE detectors when a larger number could so easily be incorporated. Why not add a flat quad detector immediately above the sample just below the lens? This would provide additional useful information.
Authors: The number of detectors used for this investigation has been held to four in order to minimize the amount of data which must be treated. We have attempted to extract a maximum amount of information from measurements made with these detectors However, either of the additional detectors suggested by the reviewers would improve the resolution of atomic number.